

1 **Quantifying the influence of agricultural fires in northwest India on urban air**
2 **pollution in Delhi, India**

4 Daniel H. Cusworth¹, Loretta J. Mickley², Melissa P. Sulprizio², Tianjia Liu¹, Miriam E.
5 Marlier³, Ruth S. DeFries⁴, and Sarath K. Guttikunda⁵

6 ¹Department of Earth and Planetary Sciences, Harvard University, Cambridge, 02138, USA

7 ²School of Engineering and Applied Sciences, Harvard University, Cambridge, 02138, USA

8 ³RAND Corporation, Santa Monica, 90401, USA

9 ⁴Department of Ecology, Evolution, and Environmental Biology, Columbia University, New
10 York, 10027, USA

11 ⁵Division of Atmospheric Sciences, Desert Research Institute, Reno, NV 89512, USA

12
13
14 **Abstract**

15 Since at least the 1980s, many farmers in northwest India have switched to mechanized
16 combine harvesting to boost efficiency. This harvesting technique leaves abundant crop residue
17 on the fields, which farmers typically burn to prepare their fields for subsequent planting. A key
18 question is to what extent the large quantity of smoke emitted by these fires contributes to the
19 already severe pollution in Delhi and across other parts of the heavily populated Indo-Gangetic
20 Plain located downwind of the fires. Using a combination of observed and modeled variables,
21 including surface measurements of PM_{2.5}, we quantify the magnitude of the influence of
22 agricultural fire emissions on surface air pollution in Delhi. We first derive the signal of regional
23 PM_{2.5} enhancements (pollution above an anthropogenic baseline) from the Delhi network of
24 surface air monitors during each post-monsoon burning season (Oct. 17 – Nov. 30) for 2012–
25 2016. We next use the Stochastic Time-Inverted Lagrangian Transport model (STILT) to
26 generate particle back-trajectories from Delhi, which allows us to map the sensitivity of Delhi
27 pollution to agricultural fires in each grid cell upwind. By combining these sensitivity maps with
28 emissions from a suite of fire inventories, we reproduce up to 25% of the weekly variability in

29 total observed PM_{2.5}. Our method attributes as much as 78% of the maximum observed PM_{2.5}
30 enhancements in Delhi to fires upwind in some years, although this contribution varies greatly by
31 year and emission inventory. The large range in these attribution estimates points to the
32 uncertainties in fire emission parameterizations, especially in regions where thick smoke may
33 interfere with hotspots of fire radiative power. Although our model can generally reproduce the
34 largest PM_{2.5} enhancements in Delhi air quality for 1-3 consecutive days each fire season, it fails
35 to capture many smaller daily enhancements, which we attribute to the challenge of detecting
36 small fires in the satellite retrieval. By quantifying the influence of upwind agricultural fire
37 emissions on Delhi air pollution, our work helps identify the health benefits of changes in
38 farming practices that reduce fires.

39

40 **1 Introduction**

41 Residents of the heavily populated Indo-Gangetic Plain (IGP) in India experience
42 elevated health risks due to poor air quality. The National Capital Territory of Delhi (hereafter
43 referred to as Delhi) sits within the IGP and has a population of ~16.5 million. The larger
44 National Capital Region of Delhi which is centered on Delhi but also includes regions of
45 Haryana, Uttar Pradesh, and Rajasthan is estimated to exceed a population of 46 million
46 (Registrar General, India, 2011). Daily mean levels of surface particulate matter (PM_{2.5})
47 pollution in Delhi often exceed the World Health Organization threshold for unhealthy air (24-
48 hour average of 25 $\mu\text{g m}^{-3}$) as well as the daily mean threshold set by the Indian Central Pollution
49 Control Board (CPCB, 60 $\mu\text{g m}^{-3}$). Delhi is often in exceedance of these standards during the
50 post-monsoon season (Oct.-Dec.), and its ambient PM_{2.5} concentrations are subject to large

51 episodic spikes. For example, from Nov. 1st – Nov. 15th, 2016, the PM_{2.5} concentration at the
52 Mandir Marg CPCB site averaged 350 $\mu\text{g m}^{-3}$, but reached as high as a daily-average of 692 μg
53 m^{-3} on Nov. 5th (<http://www.cpcb.gov.in/CAAQM/>). One major uncertainty is the extent to
54 which smoke emissions from post-monsoon agricultural fires in rural areas influence the already
55 high concentrations urban air pollution in the IGP. This study aims to quantify the magnitude of
56 the contribution of these fire emissions to PM_{2.5} pollution in Delhi during the post-monsoon
57 burning season over the 2012-2016 time frame. The attribution of surface PM_{2.5} due to fires
58 versus other anthropogenic sources is critical in developing strategies to reduce overall pollution
59 exposure.

60 Exceedances of PM_{2.5} standards in Delhi occur year-round, with an annual mean PM_{2.5}
61 concentration of more than 100 $\mu\text{g m}^{-3}$ (e.g., Twiari et al., 2013). Much of the pollution comes
62 from coal-fired power plants, transportation, and domestic combustion sources (Guttikunda and
63 Jawahar, 2014; Gurjar et al., 2016). PM_{2.5} and its precursors (e.g., SO₂, NOx) have led to an
64 estimated 30% of Delhi's population suffering from respiratory disorders (Kandlikar and
65 Ramachadran, 2000). Nagpure et al. (2014) estimated a ~60% increase in Delhi mortality due to
66 the degradation of air quality between 2000 and 2010. Residents of Delhi have been found to
67 suffer from diseases related to air pollution at a rate 12 times higher than the national average
68 (Kandlikar and Ramachadran, 2000). More broadly, Dey et al. (2012) estimated that about half
69 the subcontinent's population experienced pollution levels above the WHO PM_{2.5} annual mean
70 standard of 35 $\mu\text{g m}^{-3}$ during 2000-2015, with the greatest pollution exposure in the IGP.

71 India's agricultural “breadbasket” is located in the northwestern-most region of the
72 country, mostly in the state of Punjab but also in the neighboring state of Haryana. Agriculture

73 here is typically characterized by two growing seasons: a predominantly winter wheat crop,
74 harvested in April-May, and a predominantly summer rice crop, harvested in October-November
75 (Vadrevu et al., 2011). Increasing utilization of mechanized harvesters over the last 30 years has
76 decreased costs and improved efficiency for farmers, and studies have found that more than 75%
77 of rice is harvested using a combine harvester in Punjab (Kumar et al., 2015). However, this
78 harvesting method leaves more crop residue on the fields than more traditional methods, and
79 many farmers burn this residue to ready fields for the next growing season (Kaskaoutis et al.,
80 2014). Smoke from these fires consists of black carbon and organic particulate matter. The post-
81 monsoon rice harvest season coincides with post-monsoon conditions that favor stagnation and
82 weak surface northwesterly winds in the IGP (Singh and Kaskaoutis, 2014). These conditions
83 allow smoke to slowly permeate throughout the IGP, including Delhi, about 350 km downwind
84 from Punjab.

85 Previous work has diagnosed co-variability between fire emissions in Punjab and
86 observed urban pollution levels in the region and downwind. For example, using ground-based
87 sensors in the Punjab city of Patalia, Mittal et al. (2009) reported PM_{2.5} enhancements as high as
88 547 $\mu\text{g m}^{-3}$ during the 2007 burning season of October-November. Using remotely sensed data
89 from the Moderate Resolution Imaging Spectroradiometer (MODIS), Mishra and Shibata (2012)
90 found enhancements of 0.1-0.3 in 850-nm aerosol optical depth (AOD) during the 2009 post-
91 monsoon burning season over the IGP. These authors used lidar to probe the vertical distribution
92 of the aerosols over the Punjab and Delhi and found the largest 532-nm backscatter coefficients
93 ($>0.0035 \text{ km}^{-1} \text{ sr}^{-1}$) close to the surface (below 1.0 km altitude). Consistent with this study,
94 Kaskaoutis et al. (2014) found daily maximum MODIS 550-nm AOD to often be in excess of 2.0

95 during the 2012 post-monsoon burning season. Observations from two Aerosol Robotic Network
96 (AERONET) sites in the IGP show that aerosols tend towards larger volume and lower particle
97 size during the post-monsoon burning season (Kaskaoutis et al., 2014); such attributes are
98 characteristic of fresh soot. Our previous work (Liu et al., 2018) used back trajectory analysis to
99 define an airshed region upwind of Delhi during the burning season. The study focused on
100 relating available data on PM₁₀ and other air quality measurements to fire radiative power (FRP)
101 in the airshed for both burning seasons, accounting for meteorological conditions. We found that
102 MODIS FRP within the airshed correlates with observed concentrations of surface PM₁₀,
103 visibility, and AOD in Delhi, suggesting a coupling between upwind fires, meteorology, and
104 urban pollution.

105 Missing from recent studies is an estimate of the magnitude of surface PM_{2.5} in Delhi that
106 can be attributed to agricultural fire emissions. Building on the work of Liu et al. (2018) and
107 other studies, this study aims to address this gap by combining analysis of surface PM_{2.5}
108 observations in Delhi with chemical transport modeling. We first use daily 2012-2016 surface
109 observations to estimate the seasonal PM_{2.5} enhancement due to regional (i.e., fire) sources. We
110 compare these enhancements to model-derived PM_{2.5} driven by a suite of fire emission
111 inventories. We rely mostly on a Lagrangian-based modeling framework, which uses back
112 trajectories to simulate chemical transport and map the sensitivity of PM_{2.5} levels in Delhi to fire
113 activity upwind. We find that our model can capture much of the weekly observed PM_{2.5}
114 variability in Delhi, as well as at least some of extreme peaks in daily PM_{2.5} during the post-
115 monsoon burning season. Discrepancies between the model and observed PM_{2.5} in Delhi point
116 to the difficulty in detecting small fires from satellite, especially when clouds and/or smoke

117 interfere with detection. Smoke from satellite-detected fires that are detected can contribute more
118 than half the total observed PM_{2.5} across Delhi.

119

120 **2 Data and Methods**

121 *2.1 Surface and Satellite Observations*

122 The CPCB provides online hourly observations of a variety of pollutants including PM_{2.5}
123 at 12 sites within Delhi (<http://www.cpcb.gov.in/CAAQM>). We focus on observed PM_{2.5} during
124 the post-monsoon burning season (here defined as Oct. 17 – Nov. 30) during 2012-2016. No
125 CPCB site provides a complete record of PM_{2.5} observations during the entire course of 2012-
126 2016. The U.S. Embassy in Delhi (<http://newdelhi.usembassy.gov/airqualitydata.html>) also
127 provides daily PM_{2.5} from 2013-2016, and is mostly complete during that time span. Finally, we
128 rely on observations from a new monitoring network, #Breathe
129 (<http://api.indiaspend.org/dashboard/>), launched in 2016 by IndiaSpend, a grassroots initiative to
130 monitor air quality at 10 sites in Delhi and elsewhere in India. Figure S1 shows the spatial
131 configuration of all surface sites where PM_{2.5} was available sometime during 2012-2016. We
132 aggregate and validate these surface observations with satellite AOD (described in Section 3.1)
133 retrieved from the MODIS Level 3 Aqua Deep Blue algorithm (MYD08D3; Levy et al., 2013).
134 The Deep Blue algorithm is designed to provide AOD retrievals over bright surfaces, and was
135 found to correlate well with the AERONET station in Kanpur, India ($R = 0.86$; Sayer et al.,
136 2013).

137

138 *2.2 Fire emission inventories*

139 Few sources of *in situ* information exist that can be used to quantify regional fire
140 emissions on the daily scale in Punjab and Haryana. Thus, we consider top-down fire emission
141 inventories that are based on satellite information. As we shall see, many assumptions are needed
142 to translate the satellite retrievals into emissions. The inventories considered in this study are the
143 Fire Inventory from NCAR (FINN; Wiedinmyer et al., 2011), the Global Fire Emissions
144 Database version 4 with small fires (GFED4.1s; van der Werf et al., 2017, Giglio et al., 2013;
145 Randerson et al., 2012), the Global Fire Assimilation System (GFAS; Kaiser et al., 2012), and
146 The Quick Fire Emissions Dataset (QFED; Darmenov and da Silva, 2015). Each of these fire
147 emission inventories are based in part on thermal anomalies detected by MODIS (Giglio et al.,
148 2006). However, they each differ in their treatment of emission factors and land cover that
149 translate these thermal anomalies into emission estimates, and they also have different methods
150 for treating gaps in the MODIS record. FINN aggregates 1-km MODIS active fire detections and
151 produces a daily emission estimate given these detections and MODIS retrieved land cover.
152 GFED4.1s relies primarily on monthly MODIS 500-m burned area maps, derived from observed
153 changes in surface reflectance, to generate emission estimates. The dataset then adds 1-km active
154 fire information to incorporate the influence of small fires that may have not accounted for by the
155 burned area product (Randerson et al., 2012). GFED4.1s derives a daily emission estimate by
156 applying the ratio of daily emissions to total monthly emissions in each grid cell. GFAS also
157 aggregates the 1-km MODIS FRP and uses emission factors similar to those in GFED4.1s. To
158 account for FRP obscured by sub-grid clouds and other interferences, GFAS assumes that an
159 obscured FRP pixel is equivalent in value to its adjacent non-obscured pixel, as long as they are
160 not over a body of water (Kaiser et al., 2012). GFAS further uses a Kalman filtering method of

161 data assimilation, in which the optimal estimate of FRP for a given day is a weighted average of
162 the optimal FRP estimate from the previous day and the FRP estimate for the current day (Kaiser
163 et al., 2012). Like GFAS, QFED uses information from adjacent pixels to estimate obscured
164 thermal anomalies; QFED also relies on FRP estimates from the previous day. However, the
165 QFED algorithm weights adjacent pixel information via the error covariance between pixels, and
166 it allows the estimate of the previous day's FRP to decay according to a characteristic timescale
167 derived for each land type (Darmenov and da Silva, 2015). GFAS, QFED, and FINN are
168 available in near real time, whereas GFED4.1s requires several months of processing before
169 public release. We include another inventory, here called GFED + Agriculture. In this inventory,
170 we apply the GFED4.1s dry matter emission estimates, but assume the land cover within each
171 burning grid cell is 100% agricultural, thus enhancing burned area to its maximum amount in
172 each cell. We also increase the GFED4.1s emission factors associated with agricultural burning
173 by a factor of three. The factor of three scaling is based on the laboratory findings of Oanh et al.
174 (2010), who found that the particulate matter emissions of rice straw approximately tripled when
175 the straw was piled instead of spread evenly on the ground. The GFED + Agriculture emissions
176 thus represent a high derived upper bound on agricultural burning in the region.

177

178 *2.3 Chemical transport modeling*

179 We perform 2012-2016 simulations of daily surface PM_{2.5} in Delhi using the Stochastic
180 Time-Inverted Lagragian Transport (STILT) model (Lin et al., 2003), driven by 0.5° x 0.5°
181 Global Data Assimilation meteorology (GDAS; Houser et al., 2001). STILT is a receptor-
182 oriented Lagrangian particle dispersion model. This modeling framework has previously been

183 used to assess the influence of wildfires on urban air pollution in Salt Lake City, Utah (Mallia et
184 al., 2015). By tracing an ensemble of theoretical particles or air-mass trajectories from a receptor
185 site backwards in time, STILT computes the sensitivity of PM_{2.5} concentration at the receptor to
186 emissions in the surrounding region. The resulting flux footprint reveals those regions where
187 emissions likely influenced PM_{2.5} at the receptor. We simulate daily footprints of the sensitivities
188 of Delhi pollution to fire emissions upwind by sending 500 simultaneous air-mass trajectories
189 backwards in time for 5 days. We choose 500 ensembles in order to account for random
190 turbulence air-masses experience, especially in the boundary layer (Lin et al., 2013). We choose
191 five days as this timeframe should allow an air mass to traverse the approximately 800 km
192 between Delhi and the farthest upwind burning regions even under the weak wind conditions
193 prevalent at this time of year, which is often less than 5 m s⁻¹ according to GDAS. Figure 1
194 shows the spatial footprint of the median 2012-2016 sensitivities of a Delhi receptor (28.62N,
195 77.21E) to the surrounding emissions during the burning season. We see that Delhi is highly
196 sensitive ($\sim 10^{-3}$ ppm $\mu\text{mol}^{-1} \text{m}^2 \text{s}$) to the upwind burning regions in Punjab. Similar to Koplitz et
197 al. (2016), we assume that the PM_{2.5} reaching Delhi from upwind fires is in its primary BC or OC
198 form.

199 Liu et al. (2018) performed a back-trajectory analysis using the Hybrid Single Particle
200 Lagrangian Integrated Trajectory Model (HYSPLIT; Stein et al., 2015) to create an airshed
201 region upwind of Delhi. The boundaries of this airshed determined a region where agricultural
202 fire emissions could potentially influence downwind air pollution in Delhi. Through the use of
203 STILT, we make this relationship more explicit by quantifying explicitly how much those
204 upwind emissions contribute to a particular downwind pollution observation. In other words,

205 each STILT footprint can be coupled to an emissions inventory in order to simulate surface
206 PM_{2.5} concentrations. The footprint for the i^{th} receptor location and time can be expressed as a
207 vector $\mathbf{k}_i = (\partial y_{stilt,i} / \partial \mathbf{x})^T$, where \mathbf{x} is a vector of upwind emissions from the previous 5 days
208 (units of $\mu\text{mol m}^{-2} \text{ s}^{-1}$), and $y_{stilt,i}$ is the modeled PM_{2.5} enhancement due to those emissions. If we
209 couple this footprint to an emissions estimate (e.g., FINN, QFED, etc.) from the previous 5 days,
210 we can simulate surface PM_{2.5} enhancement from fires using the relation $y_{stilt,i} = \mathbf{k}_i \bullet \mathbf{x}$. These
211 simulated surface concentrations can then be compared to the observed network average of PM_{2.5}
212 observations.

213 We simulate the urban fate of primary PM_{2.5} from fires and assume no chemistry using
214 STILT. To account for additional PM_{2.5} production from other anthropogenic sources, we
215 determine a background or baseline from observations (described further in section 3.2). We
216 compare this baseline to a simulated anthropogenic PM_{2.5} from the 3-D global chemical transport
217 model, GEOS-Chem (geos-chem.org). GEOS-Chem is here driven by assimilated meteorological
218 data from the Goddard Earth Observing System (GEOS-5) at the NASA Global Modeling
219 Assimilation Office (GMAO). The aerosol simulation in GEOS-Chem includes sulfate, nitrate,
220 ammonium, dust, and black and organic carbon (Kim et al., 2015), and many previous studies
221 have examined PM_{2.5} pollution in Asia using GEOS-Chem (e.g., Wang et al., 2013; Mu and
222 Liao, 2014; Geng et al., 2015). Here we utilize the emission inventory for Model Inter-
223 Comparison Study for Asia (MIX) for anthropogenic aerosol precursor emissions (Li et al.,
224 2015). We follow Bond et al. (2007) for anthropogenic emissions of primary black and organic
225 carbon. For this study, we perform nested grid simulations for the 2012 burning season at 0.5° x

226 0.667° resolution over most of eastern Asia, with lateral boundary conditions provided by a
227 global simulation at 2° x 2.5° horizontal resolution.

228

229 *2.4 Statistical modeling*

230 We try improving the STILT simulation of PM_{2.5} for a certain receptor ($y_{stilt,i}$) using a
231 statistical model that relies on local variables that may not be well captured in the 0.5° reanalysis,
232 e.g., local precipitation, mixing layer height, and wind speed. Our statistical prediction of surface
233 PM_{2.5} from fires takes the form:

234
$$y_{stat,i} = \mathbf{h}_i \bullet \mathbf{w}$$

235 where \mathbf{h}_i is a $l \times d$ vector consisting of meteorological parameters and the STILT driven PM_{2.5}
236 prediction ($y_{stilt,i}$), and \mathbf{w} is a $d \times 1$ vector of coefficient weights that represent the relative
237 importance of each predictor in \mathbf{h}_i to the prediction of PM_{2.5}. The optimal value of these weights
238 is solved for empirically. For example, if we aggregate all daily observed network-averaged
239 surface observations above the anthropogenic baseline (\mathbf{y}_{obs}), the traditional ordinary least square
240 setup determines the optimal value of coefficient weights (\mathbf{w}) by the following relation:

241
$$\mathbf{w}^* = (\mathbf{H}^T \mathbf{H})^{-1} \mathbf{H}^T \mathbf{y}_{obs}$$

242 where \mathbf{H} is an $n \times d$ matrix and n is the number of observations. Each column of \mathbf{H} represents the
243 time series of daily mean values of a particular predictor. To avoid overfitting in solving for \mathbf{w}^* ,
244 we follow the method of the least absolute shrinkage and selection operator (LASSO; Tibshirani,
245 1996), which reduces the magnitude of the coefficients of correlated predictors and those
246 predictors offering little information. Here the optimal coefficients are determined through the
247 following algorithm:

248 $\mathbf{w}^* = \min_{\mathbf{w} \in \mathbb{R}^D} \{\|\mathbf{H}\mathbf{w} - \mathbf{y}_{obs}\|_2^2 + \lambda \|\mathbf{w}\|_1\}$

249 In the above equation, the first term on the right-hand side of the equation penalizes
250 mismatch between model and observations using the square loss function, hence the “2”
251 subscript. The second term of the equation regularizes the fit (i.e., reduces overfitting) by
252 penalizing the magnitude of \mathbf{w} via the absolute loss, also known as the L_1 norm, hence the “1”
253 subscript. The algorithm is optimized over a grid of λ values (to control the degree of
254 regularization), using three-fold cross validation. This method randomly separates the data into
255 three sets and fits the statistical model on two of these sets, and then these fitted coefficients are
256 applied to remaining set (called the validation set), yielding the root mean squared error (RMSE)
257 between the prediction (\mathbf{y}_{stat}) for that set and the observations (\mathbf{y}_{obs}). This process is repeated
258 three times, and the value of λ that provides the best RMSE on the reserved validation sets is
259 retained. In addition to \mathbf{y}_{stilt} , the array of local meteorological variables at Delhi used as
260 predictors include wind speed and wind direction from the surface to the boundary layer and
261 from the boundary layer to 500 hPa, as well as boundary layer height, precipitation, surface
262 temperature, and surface pressure. All variables are taken from the Integrated Global Radiosonde
263 Archive (Durre et al., 2006) and the Global Historical Climatology Network (Menne and
264 Williams, 2009). IGRA estimates boundary layer heights over the Safdarjung airport (28.58N,
265 77.2E) using the parcel method, which locates the altitude where virtual potential temperature is
266 equivalent to surface virtual potential temperature (Seibert et al., 2000).

267

268 **3 Results**

269 *3.1 Creating a network-average of PM_{2.5}*

270 Due to data inconsistencies among the CPCB sites, we employ data quality preprocessing
271 before calculating a city-wide network average of urban PM_{2.5} for Delhi. Figure 2 shows the
272 number of daily averaged PM_{2.5} observations available at each site during the burning season for
273 each year. As previously noted, the U.S. embassy data are available only for 2013-2016, and
274 IndiaSpend data only for 2016. Both data sources provide near complete measurement records
275 over these time periods. Few CPCB sites have a record of observations of more than three years
276 during 2012-2016. To represent mean pollution exposure across the city through the years, we
277 implement a two-step data-cleaning procedure. First, we compare daily averaged CPCB PM_{2.5}
278 with corresponding MODIS AOD for each site during the burning season, using all available
279 observations during 2012-2016. Then we select only those sites whose correlation with the AOD
280 timeseries exceeds $R=0.5$ and is statistically significant ($p < 0.05$). The purpose of this step is to
281 consider only those sites whose variability corresponds to regionally influenced pollution, as
282 diagnosed by MODIS AOD. Next, for each CPCB site that meets this correlation criterion, we
283 calculate the mean absolute difference of daily-averaged PM_{2.5} at that site compared to the
284 network average of daily-averaged PM_{2.5} at the other sites in the network. We also compute the
285 standard deviation of that difference across the five years. This step produces a metric revealing
286 how much daily PM_{2.5} at each site tends to deviate from PM_{2.5} at the other sites on average. We
287 find that these deviations are distributed normally, so that for any given day, if the absolute
288 difference in PM_{2.5} at a particular site deviates more than ± 2.5 standard deviations from the
289 mean absolute difference associated with that site, we exclude that PM_{2.5} observation from the
290 network average for that day. Thus for any given day, we remove from consideration those sites
291 that either experience instrument malfunction and/or appear to be heavily influenced by strong

292 local sources. For each station, we could alternatively consider removing observations that
293 deviate too much from that station's mean PM_{2.5} concentration during the post-monsoon burning
294 season. However, we have seen that surface PM_{2.5} varies widely during large fire episodes. For
295 example the Mandir Marg CPCB site observed daily-averaged surface PM_{2.5} between 120 – 692
296 µg m⁻³ during Nov. 1-15, 2016. The higher PM_{2.5} enhancements could erroneously be marked as
297 outliers from local sources and/or instrument malfunction. Therefore, we wish to consider
298 outliers as a function of the network average of monitors, as we expect all surface monitors to
299 jointly respond to the regional signal of fire emissions and transport.

300

301 *3.2 Baseline PM_{2.5} derivation during fire season*

302 We next determine a PM_{2.5} baseline in Delhi to represent typical pollution levels in the
303 absence of smoke from agricultural fires. This baseline represents the mean anthropogenic
304 contribution to total PM_{2.5} during the post-monsoon burning season. Quantification of this
305 baseline is important as we use it to derive a PM_{2.5} enhancement from observations (y_{obs} = total
306 observed PM_{2.5} – baseline). Baseline anthropogenic PM_{2.5} in post-monsoon months consists of
307 elemental carbon, organic matter, and secondary sulfate-nitrate-ammonium from gasoline
308 exhaust, coal combustion, dust, and urban biomass combustion (Pant et al., 2015). For simplicity,
309 we assume that baseline levels are constant during a given burning season. However, we
310 anticipate that baseline PM_{2.5} likely changes over the years due to changes in the surface
311 monitoring network and local emission sources. For these reasons, we compute a unique baseline
312 PM_{2.5} for each year during 2012-2016. We apply three different methods with different
313 assumptions in order to test the robustness of our baseline estimates.

- 314 • Method 1: This method relies on the daily variability of the GFAS fire emissions. We
315 choose GFAS due to its assimilation properties which account some missing or obscured
316 fire pixels. For each fire season, we analyze the time series of these emissions summed
317 over all grid cells in the burning regions upwind of Delhi. We specify low-fire days as
318 those days when total fire emissions fall below a specified threshold at the low end of the
319 frequency distribution for that season – e.g., below the 10th percentile. On days when fire
320 emissions fall below that threshold, we assume that Punjab and Haryana are not burning
321 significantly. If emissions remain below the threshold during the next N days, we tag the
322 observation for that N^{th} day as representative of the baseline. The baseline is then the
323 average of all tagged days during the fire season. We vary N between 1-5 and the
324 emission percentile threshold between 10-30% to check the robustness of our baseline
325 estimate. We assume that N represents the transport time for smoke from fires to ventilate
326 out of the IGP.
- 327 • Method 2: In this method, we take advantage of STILT sensitivity estimates. For each
328 day of the fire season, STILT provides gridded sensitivities to upwind emissions for each
329 observation in Delhi. If the map of sensitivity overlaps with cells containing fire
330 emissions, the model predicts a pollution enhancement due to fire downwind in Delhi in
331 the subsequent days. To compute the anthropogenic baseline, we count the number of fire
332 emitting pixels for a particular day. We then count the number of those fire pixels that
333 overlap with the STILT sensitivity map. If the ratio of overlapping pixels to total fire
334 pixels is sufficiently low (e.g., less than a threshold of 0.1) on a given day, we assume
335 that the urban pollution for that day has little influence from fires. We collect each of

336 these non-fire days during each fire season and take their average as the baseline. We
337 vary the ratio threshold between 0.1-0.7 to assess the sensitivity of this method to its
338 underlying assumptions.

- 339 • Method 3: For this method, we compute the weekly block average of PM_{2.5} within the
340 city for each week (Sunday through Saturday) of the burning season. We then average the
341 M lowest weekly averages to determine the baseline. We vary M between 1-4 to check
342 the sensitivity of this method to this parameter.

343

344 Figure 3 shows the interannual variability in baseline estimates of urban pollution in
345 Delhi for 2012-2016. Depending on the year and method chosen, the baseline can vary from 130
346 - 290 $\mu\text{g m}^{-3}$. The Method 3 baseline is consistently lower than the other baselines, however each
347 baseline estimate is at least twice the CPCB daily air quality standard of 60 $\mu\text{g m}^{-3}$. Method 3
348 shows the greatest interannual stability, and predicts an average baseline across 2012-2016 of
349 about 150 $\mu\text{g m}^{-3}$, which is within the annual average range of $122.3 \pm 90.7 \mu\text{g m}^{-3}$ total PM_{2.5}
350 reported by Twiari et al. (2013) for Delhi in 2011.

351 We compare these baseline estimates of Delhi PM_{2.5} to that provided by GEOS-Chem.
352 For this comparison, we perform the GEOS-Chem simulation with emissions from agricultural
353 fires turned off. Figure S2 shows the resulting distribution of daily average urban PM_{2.5} during
354 the burning season of 2012. The distribution is centered on a mean of 99 $\mu\text{g m}^{-3}$, but is slightly
355 skewed towards larger PM_{2.5} values, with a maximum at 200 $\mu\text{g m}^{-3}$. Our observation-driven
356 method for determining the 2012 PM_{2.5} baseline yields values ranging from $165 \pm 12.5 \mu\text{g m}^{-3}$ to
357 $196 \pm 14.7 \mu\text{g m}^{-3}$ (Figure 3), or about 1.6–2 times the mean GEOS-Chem simulated baseline.

358

359 *3.3 Variability of surface PM_{2.5}*

360 We first probe how well the STILT modeling framework reproduces the variability of
361 PM_{2.5} in Delhi during the burning season. Our approach is to couple daily STILT sensitivity maps
362 to each of the fire emission inventories described in Section 2.2 and compare the resulting PM_{2.5}
363 enhancements in Delhi to those observed when averaged across the network and with the derived
364 PM_{2.5} baseline subtracted. To reduce noise and variability arising from local emissions, we
365 consider only weekly-averaged modeled and observed PM_{2.5} enhancements. Results show that
366 each of the emission inventories to some degree captures the variability in the surface observed
367 surface PM_{2.5} ($0.29 < R < 0.50$, Table 1), suggesting that smoke from fires upwind drives at least
368 part of the weekly variability of Delhi PM_{2.5}. This modeling result agrees with previous studies
369 that report significant correlations between urban AOD, PM₁₀, visibility, and PM_{2.5} and MODIS
370 FRP (Liu et al., 2018; Kaskaoutis et al., 2014).

371 As a measure of the mean bias of our predicted PM_{2.5} compared to Delhi observations,
372 we compute the RMSE (Table 1). We find that driving the model with STILT alone accounts for
373 an RMSE between $79 - 109 \mu\text{g m}^{-3}$, depending on the baseline method and emissions inventory,
374 revealing that even though we can predict much of the observed surface PM_{2.5} variability using
375 STILT, we greatly underestimate the magnitude of the enhancements. A potential reason for this
376 underestimate could be that the GDAS reanalysis used to drive STILT poorly characterizes the
377 local meteorology. We add information from local meteorological sources and fit a statistical
378 model to the observed PM_{2.5} enhancements. Results of the statistical model are shown in Table 1.
379 Adding local meteorological factors improves the correlation of predicted vs. observed PM_{2.5} in

380 each fire emission scenario ($0.66 < R < 0.78$). Figure 4 presents the normalized regression
381 coefficient weights for just the GFED4.1s simulation. Regression coefficients for other statistical
382 models fit with different emission inventories are shown in Figure S3. The STILT-GFED4.1s
383 predictor is one of the most significant contributors, as expected by the presence of significant
384 correlation ($0.43 < R < 0.50$) between observed and GFED4.1s STILT-derived PM_{2.5}
385 enhancements. The next two dominant predictors of observed PM_{2.5} are wind speed below the
386 boundary layer. This result underscores the importance of local meteorology as drivers of urban
387 PM_{2.5} variability and suggests that the assimilated GDAS meteorology may not capture such
388 meteorological effects at 0.5° resolution. The statistical model yields RMSE values ranging from
389 53 – 68 µg m⁻³, substantially lower than those from the purely STILT driven model, but still
390 rather large. We hypothesize that other unaccounted factors (e.g., the smoke from small fires
391 that escape satellite detection) could lead to model bias. We discuss this reasoning further in
392 Section 4.

393

394 *3.4 Maximum daily enhancement of PM_{2.5} during burning season*

395 While we capture the variability of PM_{2.5} with both STILT and the statistical model, in
396 both bases we find a high RMSE when compared to observations. Here we focus on smoke
397 extremes during each fire season to probe whether the model systematically underestimates
398 surface PM_{2.5}. We also quantify the contribution of smoke PM_{2.5} derived from observations or
399 STILT (\mathbf{y}_{obs} or $\mathbf{y}_{\text{stilt}}$, respectively) to total PM_{2.5} during these extreme events.

400 Figure 5 shows the model simulated maximum daily smoke enhancement in each burning
401 season – i.e., the enhancement on that day each season characterized by the greatest simulated

402 PM_{2.5} value. For years where STILT simulations disagree on which day should produce maximal
403 PM_{2.5}, we choose the day where most models agree. The plot also shows the observed PM_{2.5}
404 enhancement and total observed PM_{2.5} that correspond to the day where the STILT simulation
405 predicted the maximal urban pollution enhancement. We compare these values in Figure 5 to the
406 maximum observed PM_{2.5} enhancement for each burning season, regardless of when the STILT
407 simulation predicted a large enhancement. The largest observed PM_{2.5} enhancements occur in
408 2012 and 2016 (492 and 648 $\mu\text{g m}^{-3}$ respectively, averaged across all baseline methods). The
409 maximum observed enhancements are much lower during 2013-2015 (130-264 $\mu\text{g m}^{-3}$), which
410 could be a result of lower fire activity or other local pollution-causing events. The magnitude
411 and interannual variability in the maximum observed PM_{2.5} enhancement differs from STILT,
412 where the largest simulated PM_{2.5} enhancement occurs in 2013 (65-232 $\mu\text{g m}^{-3}$). The STILT
413 simulated enhancements show roughly interannual consistency during 2012-2016 when averaged
414 across all inventories (99-160 $\mu\text{g m}^{-3}$). However, several of the days over 2012-2016 where the
415 observations alone predict the largest seasonal enhancements are not consistent with the days
416 STILT predicts. When we instead compare the maximum STILT enhancements to the same-day
417 corresponding observed PM_{2.5} enhancement (108-299 $\mu\text{g m}^{-3}$), we find closer agreement, though
418 the observations still show more interannual variability than STILT. The FINN and GFED +
419 Agriculture emission inventories often give the largest estimate of magnitude of the observed
420 PM_{2.5} enhancement in Delhi (145-231 $\mu\text{g m}^{-3}$ and 147-255 $\mu\text{g m}^{-3}$, respectively). We find the
421 largest mismatch between observed and modeled enhancements during 2012 and 2016 across all
422 models, when we expect the largest enhancement of PM_{2.5} due to fires. In these years, depending
423 on emission inventory, the maximum STILT derived enhancements are 45-147 and 37-255 $\mu\text{g m}^{-3}$

424 m^{-3} , respectively. We see large variability across emission inventories in their ability to capture the
425 observed maximum daily enhancement of $\text{PM}_{2.5}$, and we find that the standard deviation across
426 modeled enhancements for a given year during 2012-2016 ranges between 50-91 $\mu\text{g m}^{-3}$.

427 Table 2 shows the percent contributions of smoke $\text{PM}_{2.5}$ to total $\text{PM}_{2.5}$ on extreme smoke
428 days predicted by STILT – i.e., the day during the season where STILT predicts that the smoke
429 enhancement is greatest. This provides a metric of the contribution of fires during the largest
430 predicted episodes each season to total surface particulate pollution observed in Delhi. The
431 observed $\text{PM}_{2.5}$ enhancement on days where STILT predicted a pollution maximum accounts for
432 21-72% of the total observed $\text{PM}_{2.5}$, depending on the year and baseline method used, implying
433 that $\text{PM}_{2.5}$ from a regional source (here assumed to be fires) can constitute a large fraction of the
434 total $\text{PM}_{2.5}$ concentration. For STILT $\text{PM}_{2.5}$, the GFED + Agriculture and FINN simulations
435 provide large $\text{PM}_{2.5}$ estimates, and can account for as much as 78% and 68% percent
436 (respectively) of the total corresponding observed $\text{PM}_{2.5}$ in 2014, and 40-62% and 28-54% in the
437 other years, respectively. This result means that on days where STILT predicts a large
438 enhancement in Delhi from agricultural fires, the smoke from these fires constitutes a large
439 portion of the total $\text{PM}_{2.5}$. On the lower end, the GFAS simulation accounts for just 7.0-24% of
440 the corresponding total $\text{PM}_{2.5}$. Since all inventories use MODIS fire detections to constrain
441 emissions, the variability in $\text{PM}_{2.5}$ estimates that arise from these inventories can be attributed to
442 differing emission factors, allocation of additional fires from burned area maps, model
443 assimilation, and MODIS gap-filling methods. Figure 5 and Tables 1-2 show the large sensitivity
444 in our $\text{PM}_{2.5}$ estimates to the underlying assumptions used to translate satellite retrievals to actual
445 emissions.

446 The results of Figure 5 and Table 2 show that STILT can reproduce much of the observed
447 $\text{PM}_{2.5}$ enhancement in Delhi (depending on the emission inventory used), which conflicts with
448 the high RMSE between observed and modeled enhancements in Table 1. To further investigate
449 the reasons driving the discrepancies between observed and modeled $\text{PM}_{2.5}$ enhancements, we
450 plot a sample time series of observed and simulated $\text{PM}_{2.5}$ enhancements for the 2013 post-
451 monsoon burning season (Figure 6). Three versions of the STILT model – those driven by
452 FINN, QFED, and GFED + Agriculture emissions – are able to match the $\text{PM}_{2.5}$ enhancement on
453 November 5th almost exactly. However, during the days before and after this large pollution
454 enhancement, these models predict little or no $\text{PM}_{2.5}$.

455 There are several potential reasons for the mismatches between modeled and observed
456 enhancements in smoke $\text{PM}_{2.5}$. On the days preceding the Nov. 5th maximum, MODIS may have
457 been unable to detect many small agricultural fires upwind. Only when a sufficient number of
458 these small fires become detectable is a pollution enhancement predicted by the STILT model.
459 The challenge in detecting small fires from satellites is a well-known problem (Randerson et al.,
460 2012). November 3rd was also the start of Diwali in 2013, a Hindu religious celebration
461 associated with an abundance of firecrackers and sparklers. Without controlling for other factors,
462 Singh et al. (2009) found PM_{10} concentrations to increase by a factor of 2-6 before and after
463 Diwali in Delhi during 2002-2007, and found the effect to be strongest at night. In Figure 6, Nov.
464 3rd total $\text{PM}_{2.5}$ is observed to be especially high ($338 \mu\text{g m}^{-3}$), however, the STILT model
465 simulations predict a small, near-zero $\text{PM}_{2.5}$ enhancement and the observed AOD is also
466 relatively low. Instead of lack of small fire detections, an alternative explanation for the
467 observed/modeled $\text{PM}_{2.5}$ mismatch on Nov. 3rd could instead be the effects of Diwali, which may

468 not be captured in fire emission inventories and the coarser AOD product. Diwali generally
469 occurs during the post-monsoon season, though not always during peak agricultural burning. In
470 Figure S4, we show the post-monsoon time series of observed and modeled PM_{2.5} for 2012,
471 2014-2016. In 2012, Diwali occurred a week after peak burning and peak observed PM_{2.5}. In
472 2016, Diwali occurred a week before peak burning and peak observed PM_{2.5}. Though Diwali
473 lasts a week, most firecrackers are lit on the first night of the festival (Singh et al., 2009). Though
474 potentially a factor in 2013, the incongruous timing of post-monsoon burning and Diwali during
475 these seasons implies that observed PM_{2.5} results from Figure 5 and Table 2 may sometimes be
476 influenced, but are not driven principally by Diwali.

477 Returning to Figure 6, for the days succeeding the Nov. 5th, 2013 PM_{2.5} enhancement,
478 local meteorology may have deviated from the coarser 0.5° GDAS winds, favoring increased
479 stagnation within the city and potentially amplifying surface PM_{2.5} exposure. Stagnation could
480 have been further amplified by boundary layer stabilization from enhanced PM_{2.5} aloft, a
481 feedback detected previously in Nanjing, China (Petaja et al., 2016).

482 We also hypothesize that dense smoke from fires may sometimes obscure the signal of
483 fire activity at the earth's surface. Figure 7a shows True Color Terra reflectance imagery from
484 MODIS as well as MODIS Aqua + Terra fire detections on a sample day over the IGP
485 (November 6, 2016). Figure 7b shows the Visible Infrared Imaging Radiometer Suite (VIIRS)
486 reflectance imagery with VIIRS fire detections. VIIRS detects many more fires on this day than
487 does MODIS, perhaps because VIIRS has a finer resolution and different fire detection algorithm
488 than (375 m compared to 1 km; Schroeder et al., 2014). The MODIS cloud product misidentifies
489 the thick smoke plumes over the Punjab as clouds on this day. The Collection 6 MODIS fire

490 product accounts for thick smoke from fires by relaxing the thresholds that determine whether a
491 pixel is cloud-obscured (Giglio et al., 2016). In fact, for the Nov. 6th, 2016 fires in Figure 7, the
492 MODIS fire product assumes that no pixels over Punjab and Haryana are obscured by clouds,
493 even though the MODIS cloud product determines cloud cover (Figure 7c). However, fire
494 detections still appear minimal in regions where the smoke is thickest. Thus we conjecture that
495 the large model underestimates of smoke PM_{2.5} enhancements in 2016 may be due in large part
496 to layers of dense smoke interfering with satellite detection of thermal anomalies.

497

498 **4 Discussion**

499 We estimate the contribution of smoke from upwind agricultural fire emissions to PM_{2.5}
500 exposure in Delhi during the burning season (October 17 - November 30). We apply two
501 methods: (1) an observationally based method using CPCB and other surface observations, in
502 which we determine daily enhancements above background levels, averaged over Delhi, and (2)
503 application of the Lagrangian particle dispersion model STILT, in which we implement a suite of
504 fire emission inventories. We find that the two approaches yield timeseries of weekly-averaged
505 PM_{2.5} that correlate significantly ($0.29 < R < 0.50$) with each other, implying that smoke from
506 agricultural fires upwind accounts for much of the weekly variability of PM_{2.5} in Delhi during
507 the burning season. Addition of local meteorological factors (precipitation, wind speed, wind
508 direction, temperature, and mixing heights) improves the correlation further ($0.66 < R < 0.78$).
509 The maximum PM_{2.5} smoke concentration calculated by the STILT model during each burning
510 season is of similar magnitude as its corresponding observed PM_{2.5} enhancement. For example,
511 in 2013, the maximum simulated PM_{2.5} enhancements (occurring on Nov. 5th) from GFED +

512 Agriculture, QFED, and FINN are 48%, 45%, and 54% of the corresponding observed maximum
513 PM_{2.5}, respectively, close to the 54-61% range derived from observations (Table 2). This result
514 implies that smoke from agricultural fires contributes significantly to PM_{2.5} pollution in Delhi
515 during intense episodes. However, in general, the PM_{2.5} simulations greatly underestimate the
516 enhancements implied by the observations over the entire burning season, with RMSE of 79 –
517 109 µg m⁻³, indicating that further improvements to fire emission inventories are needed.

518 We find that although we can predict the magnitude of the maximum PM_{2.5} enhancement
519 during most seasons using STILT, we miss many smaller PM_{2.5} enhancements. In the case of
520 2013, many smaller fires were likely undetected due to limitations in the resolution of the
521 MODIS retrieval. Active fire detection using higher resolution (375m) VIIRS data may provide a
522 promising new avenue to quantify the contribution from small fires. For other fire seasons, as in
523 2016, STILT underestimates the maximum PM_{2.5} enhancement more severely, even though
524 Delhi experiences much greater concentrations of PM_{2.5} compared to previous seasons. The fires
525 in 2016 were especially strong, but analysis of visual MODIS imagery, fire counts, and cloud
526 cover suggests that many fires were either missed due to the coarse resolution of MODIS
527 detection or were not observed by satellites due to interference of thick smoke. Collection 6 of
528 MODIS FRP accounts for thick smoke in its algorithm by relaxing the cloud-obscuring
529 threshold, which means that regions of thick smoke where no thermal anomalies are detected
530 may now be considered unburned instead of cloud-obscured. If there are missed fires due to the
531 interaction of thick smoke with surface thermal anomalies, this could potential represent a large
532 source of underestimation in assimilated fire emission inventories. As GFAS and QFED estimate
533 FRP in cloud-obscured pixels by using information from adjacent non-obscured pixels, an

534 omitted or false-negative thermal anomaly under thick smoke would not be assimilated in the fire
535 emission inventory. In Punjab and Haryana, where thick smoke is prevalent during the post-
536 monsoon season is common due to agricultural fires and low boundary layers, this problem could
537 particularly exacerbate low fire emission estimates.

538 Much of the uncertainty in this analysis pertains to the methods of obtaining a seasonal
539 PM_{2.5} baseline. We incorporate three different methods to isolate the PM_{2.5} enhancement due to
540 fires. However, each of these methods shows considerable sensitivity to its various threshold
541 parameters, and there is much variability between each of the methods (e.g., the baseline for
542 2016 ranges from 140 to 240 $\mu\text{g m}^{-3}$). As more monitors become available in Delhi,
543 distinguishing a regional signal from local enhancement will become less challenging. Inversion
544 methods to optimize emission factors or the spatial allocation of emissions could then be applied
545 with more confidence, since these methods rely on the accuracy of the observed PM_{2.5}
546 enhancement. Instead of computing the baseline from the observations, one could instead
547 simulate the PM_{2.5} baseline using a chemistry model like GEOS-Chem over the entire time
548 domain. However, the result of such simulations would depend strongly on the quality of the
549 emissions used to drive the model. In our 2012 simulation using GEOS-Chem, we find that the
550 model underestimates the PM_{2.5} baseline by at least a factor of 2, compared to the baselines
551 derived from observations.

552 Another shortcoming of this study is our designation of the whole of Delhi as a one-point
553 receptor in the STILT simulations. With a denser network of PM_{2.5} monitors, we could further
554 simulate the variability of PM_{2.5} exposure due to fires within the city. This approach would also
555 require higher resolution meteorology than the 0.5° resolution used here.

556 Many studies have assessed the human health impact of elevated particulate pollution in
557 Delhi (Nagpure et al., 2014; Kandlikar and Ramachadran, 2000). Our work builds on these
558 studies by quantifying the contribution of agricultural burning in the Punjab and Haryana to the
559 degradation of Delhi air quality. Although officially banned nationally and enforced on the state
560 level by the National Green Tribunal Act of 2010 (Nain Gill, 2010), the practice of agricultural
561 burning is cheap and commonplace for farmers after harvest. India's population is expected to
562 surpass China 2022, and reach 1.7 billion by 2050 (United Nations, 2015). Delhi is projected to
563 grow to a population of 36 million by 2050 (Hoornweg and Pope, 2014). Thus the need for
564 efficient and cheap agricultural production is paramount to feeding the increasing population.
565 However, the adverse effects of fire emissions need to continue to be considered and more
566 accurately quantified as Delhi and the greater IGP's populations continue to grow, leaving more
567 people at risk. Building off the approaches in previous studies (e.g., Liu et al., 2018), the
568 modeling approach presented in this paper can be used to infer not just the co-variability of urban
569 pollution and upwind fires, but also the percent contribution of smoke to the already intense
570 urban PM_{2.5} in Delhi. This addition can provide policymakers with a quantitative sense of the
571 consequences of current agricultural burning practices in regions upwind of the city. As
572 estimates of fire emissions improve and the distribution of air quality monitors in Delhi expands,
573 such an approach will reduce uncertainty in the results.

574

References

- Bond, T. C., Bhardwaj, E., Dong, R., Jogani, R., Jung, S., Roden, C., Streets, D. G., and Trautmann, N. M.: Historical emissions of black and organic carbon aerosol from energy-related combustion, 1850–2000, *Global Biogeochemical Cycles*, 21, 2007.
- Darmenov, A. and da Silva, A.: The quick fire emissions dataset (QFED)—documentation of versions 2.1, 2.2 and 2.4, NASA Technical Report Series on Global Modeling and Data Assimilation, NASA TM-2013-104606, 32, 183, 2013.
- Dey, S., Di Girolamo, L., van Donkelaar, A., Tripathi, S., Gupta, T., and Mohan, M.: Variability of outdoor fine particulate (PM 2.5) concentration in the Indian subcontinent: a remote sensing approach, *Remote Sensing of Environment*, 127, 153–161, 2012.
- Durre, I., Vose, R. S., and Wuertz, D. B.: Overview of the integrated global radiosonde archive, *Journal of Climate*, 19, 53–68, 2006.
- Geng, G., Zhang, Q., Martin, R. V., van Donkelaar, A., Huo, H., Che, H., Lin, J., and He, K.: Estimating long-term PM 2.5 concentrations in China using satellite-based aerosol optical depth and a chemical transport model, *Remote Sensing of Environment*, 166, 262–270, 2015.
- Giglio, L., Csiszar, I., and Justice, C. O.: Global distribution and seasonality of active fires as observed with the Terra and Aqua Moderate Resolution Imaging Spectroradiometer (MODIS) sensors, *Journal of geophysical research: Biogeosciences*, 111, 2006.
- Giglio, L., Randerson, J. T., and Werf, G. R.: Analysis of daily, monthly, and annual burned area using the fourth-generation global fire emissions database (GFED4), *Journal of Geophysical Research: Biogeosciences*, 118, 317–328, 2013.
- Giglio, L., Schroeder, W., and Justice, C. O.: The collection 6 MODIS active fire detection algorithm and fire products, *Remote Sensing of Environment*, 178, 31–41, 2016.
- Gupta, P. K., Sahai, S., Singh, N., Dixit, C., Singh, D., Sharma, C., Tiwari, M., Gupta, R. K., and Garg, S.: Residue burning in rice–wheat cropping system: Causes and implications, *Current science*, pp. 1713–1717, 2004.
- Gurjar, B., Ravindra, K., and Nagpure, A. S.: Air pollution trends over Indian megacities and their local-to-global implications, *Atmospheric Environment*, 142, 475–495, 2016.
- Guttikunda, S. K. and Jawahar, P.: Atmospheric emissions and pollution from the coal-fired thermal power plants in India, *Atmospheric Environment*, 92, 449–460, 2014.
- Hoornweg, D. and Pope, K.: Socioeconomic pathways and regional distribution of the world's 101 largest cities, Tech. rep., Global Cities Institute Working Paper, 2013.
- Kaiser, J., Heil, A., Andreae, M., Benedetti, A., Chubarova, N., Jones, L., Morcrette, J.-J., Razinger, M., Schultz, M., Suttie, M., et al.: Biomass burning emissions estimated with a global fire assimilation system based on observed fire radiative power, *Biogeosciences*, 9, 527, 2012.

Kandlikar, M. and Ramachandran, G.: The causes and consequences of particulate air pollution in urban India: a synthesis of the science, *Annual review of energy and the environment*, 25, 629–684, 2000.

Kaskaoutis, D., Kumar, S., Sharma, D., Singh, R. P., Kharol, S., Sharma, M., Singh, A., Singh, S., Singh, A., and Singh, D.: Effects of crop residue burning on aerosol properties, plume characteristics, and long-range transport over northern India, *Journal of Geophysical Research: Atmospheres*, 119, 5424–5444, 2014.

Kim, P. S., Jacob, D. J., Fisher, J. A., Travis, K., Yu, K., Zhu, L., Yantosca, R. M., Sulprizio, M., Jimenez, J. L., Campuzano-Jost, P., et al.: Sources, seasonality, and trends of southeast US aerosol: an integrated analysis of surface, aircraft, and satellite observations with the GEOS-Chem chemical transport model, *Atmospheric Chemistry and Physics*, 15, 10411–10433, 2015.

Koplitz, S. N., Mickley, L. J., Marlier, M. E., Buonocore, J. J., Kim, P. S., Liu, T., Sulprizio, M. P., DeFries, R. S., Jacob, D. J., Schwartz, J., et al.: Public health impacts of the severe haze in Equatorial Asia in September–October 2015: demonstration of a new framework for informing fire management strategies to reduce downwind smoke exposure, *Environmental Research Letters*, 11, 094023, 2016.

Kumar, P., Kumar, S., and Joshi, L.: Socioeconomic and environmental implications of agricultural residue burning: a case study of Punjab, India, Springer, 2015.

Levy, R., Mattoo, S., Munchak, L., Remer, L., Sayer, A., Patadia, F., and Hsu, N.: The Collection 6 MODIS aerosol products over land and ocean, *Atmospheric Measurement Techniques*, 6, 2989, 2013.

Li, M., Zhang, Q., Kurokawa, J.-i., Woo, J.-H., He, K., Lu, Z., Ohara, T., Song, Y., Streets, D. G., Carmichael, G. R., et al.: MIX: a mosaic Asian anthropogenic emission inventory under the international collaboration framework of the MICS-Asia and HTAP, *Atmospheric Chemistry and Physics*, 17, 935, 2017.

Lin, J., Gerbig, C., Wofsy, S., Andrews, A., Daube, B., Davis, K., and Grainger, C.: A near-field tool for simulating the upstream influence of atmospheric observations: The Stochastic Time-Inverted Lagrangian Transport (STILT) model, *Journal of Geophysical Research: Atmospheres*, 108, 2003.

Liu, T., Marlier, M. E., DeFries, R. S., Westervelt, D. M., Xia, K. R., Fiore, A. M., Mickley, L. J., Cusworth, D. H., and Milly, G.: Seasonal impact of regional outdoor biomass burning on air pollution in three Indian cities: Delhi, Bengaluru, and Pune, *Atmospheric Environment*, 172, 83 – 92, 2018.

Mallia, D., Lin, J., Urbanski, S., Ehleringer, J., and Nehrkorn, T.: Impacts of upwind wildfire emissions on CO, CO₂, and PM_{2.5} concentrations in Salt Lake City, Utah, *Journal of Geophysical Research: Atmospheres*, 120, 147–166, 2015.

- Menne, M., Durre, I., Korzeniewski, B., McNeal, S., Thomas, K., Yin, X., Anthony, S., Ray, R., Vose, R., Gleason, B., et al.: Global historical climatology network-daily (GHCN-Daily), Version 3, NOAA National Climatic Data Center, 2012.
- Mishra, A. K. and Shibata, T.: Synergistic analyses of optical and microphysical properties of agricultural crop residue burning aerosols over the Indo-Gangetic Basin (IGB), *Atmospheric environment*, 57, 205–218, 2012.
- Mittal, S. K., Singh, N., Agarwal, R., Awasthi, A., and Gupta, P. K.: Ambient air quality during wheat and rice crop stubble burning episodes in Patiala, *Atmospheric Environment*, 43, 238–244, 2009.
- Mu, Q. and Liao, H.: Simulation of the interannual variations of aerosols in China: role of variations in meteorological parameters, *Atmospheric Chemistry and Physics*, 14, 9597–9612, 2014.
- Nagpure, A. S., Gurjar, B. R., and Martel, J.: Human health risks in national capital territory of Delhi due to air pollution, *Atmospheric Pollution Research*, 5, 371–380, 2014.
- Nain Gill, G.: A Green Tribunal for India, *Journal of Environmental Law*, 22, 461–474, 2010.
- Oanh, N. T. K., Ly, B. T., Tipayarom, D., Manandhar, B. R., Prapat, P., Simpson, C. D., and Liu, L.-J. S.: Characterization of particulate matter emission from open burning of rice straw, *Atmospheric Environment*, 45, 493–502, 2011.
- Pant, P., Shukla, A., Kohl, S. D., Chow, J. C., Watson, J. G., and Harrison, R. M.: Characterization of ambient PM_{2.5} at a pollution hotspot in New Delhi, India and inference of sources, *Atmos. Environ.*, 109, 178–189, 2015.
- Park, R. J., Jacob, D. J., Chin, M., and Martin, R. V.: Sources of carbonaceous aerosols over the United States and implications for natural visibility, *Journal of Geophysical Research: Atmospheres*, 108, 2003.
- Park, R. J., Jacob, D. J., Field, B. D., Yantosca, R. M., and Chin, M.: Natural and transboundary pollution influences on sulfate-nitrate-ammonium aerosols in the United States: Implications for policy, *Journal of Geophysical Research: Atmospheres*, 109, 2004.
- Petäjä, T., Järvi, L., Kerminen, V.-M., Ding, A., Sun, J., Nie, W., Kujansuu, J., Virkkula, A., Yang, X., Fu, C., et al.: Enhanced air pollution via aerosol-boundary layer feedback in China, *Scientific reports*, 6, 2016.
- Randerson, J., Chen, Y., Werf, G., Rogers, B., and Morton, D.: Global burned area and biomass burning emissions from small fires, *Journal of Geophysical Research: Biogeosciences*, 117, 2012.
- Registrar General, I.: Census of India 2011: provisional population totals-India data sheet, Office of the Registrar General Census Commissioner, India. Indian Census Bureau, 2011.

Rodell, M., Houser, P., Jambor, U., Gottschalck, J., Mitchell, K., Meng, C., Arsenault, K., Cosgrove, B., Radakovich, J., Bosilovich, M., et al.: The global land data assimilation system, *Bulletin of the American Meteorological Society*, 85, 381–394, 2004.

Sayer, A., Hsu, N., Bettenhausen, C., and Jeong, M.-J.: Validation and uncertainty estimates for MODIS Collection 6 ?Deep Blue? aerosol data, *Journal of Geophysical Research: Atmospheres*, 118, 7864–7872, 2013.

Schroeder, W., Oliva, P., Giglio, L., and Csizar, I. A.: The New VIIRS 375m active fire detection data product: Algorithm description and initial assessment, *Remote Sensing of Environment*, 143, 85–96, 2014.

Seibert, P., Beyrich, F., Gryning, S.-E., Joffre, S., Rasmussen, A., and Tercier, P.: Review and intercomparison of operational methods for the determination of the mixing height, *Atmospheric environment*, 34, 1001–1027, 2000.

Singh, D., Gadi, R., Mandal, T., Dixit, C., Singh, K., Saud, T., Singh, N., and Gupta, P. K.: Study of temporal variation in ambient air quality during Diwali festival in India, *Environmental monitoring and assessment*, 169, 1–13, 2010.

Singh, R. P. and Kaskaoutis, D. G.: Crop residue burning: a threat to South Asian air quality, *Eos, Transactions American Geophysical Union*, 95, 333–334, 2014.

Stein, A., Draxler, R. R., Rolph, G. D., Stunder, B. J., Cohen, M., and Ngan, F.: NOAA? s HYSPLIT atmospheric transport and dispersion modeling system, *Bulletin of the American Meteorological Society*, 96, 2059–2077, 2015.

Tibshirani, R.: Regression shrinkage and selection via the lasso, *Journal of the Royal Statistical Society. Series B (Methodological)*, pp. 267–288, 1996.

Tiwari, S., Srivastava, A., Bisht, D., Parmita, P., Srivastava, M. K., and Attri, S.: Diurnal and seasonal variations of black carbon and PM 2.5 over New Delhi, India: influence of meteorology, *Atmospheric Research*, 125, 50–62, 2013.

United Nations: World population prospects: The 2015 revision, United Nations Publications, 2015.

Vadrevu, K. P., Ellicott, E., Badarinath, K., and Vermote, E.: MODIS derived fire characteristics and aerosol optical depth variations during the agricultural residue burning season, north India, *Environmental pollution*, 159, 1560–1569, 2011.

Van Der Werf, G. R., Randerson, J. T., Giglio, L., Van Leeuwen, T. T., Chen, Y., Rogers, B. M., Mu, M., Van Marle, M. J., Morton, D. C., Collatz, G. J., et al.: Global fire emissions estimates during 1997–2016, *Earth System Science Data*, 9, 697, 2017.

Wang, Y., Zhang, Q., He, K., Zhang, Q., and Chai, L.: Sulfate-nitrate-ammonium aerosols over China: response to 2000–2015 emission changes of sulfur dioxide, nitrogen oxides, and ammonia, *Atmospheric Chemistry and Physics*, 13, 2635–2652, 2013.

Wiedinmyer, C., Akagi, S., Yokelson, R. J., Emmons, L., Al-Saadi, J., Orlando, J., and Soja, A.: The Fire INventory from NCAR (FINN): a high resolution global model to estimate the emissions from open burning, Geoscientific Model Development, 4, 625, 2011.

Table 1: Correlation and root mean squared error (RMSE) between modeled and observed PM_{2.5} enhancements in Delhi for 2012-2016. Ranges are determined by the method (1-3) used to determine the anthropogenic baseline (see section 3.1).

Model	STILT¹	STILT + LASSO²		
	<u>Correlation</u>	<u>RMSE</u>	<u>Correlation</u>	<u>RMSE</u>
GFED	0.43 – 0.50	80 - 109	0.72 – 0.78	53 - 62
QFED	0.41 – 0.46	79 – 101	0.69 – 0.72	59 - 65
FINN	0.29 – 0.45	80 – 98	0.70 – 0.73	59 – 64
GFAS	0.38 – 0.42	81 - 109	0.66 – 0.70	62 - 68

¹Correlation and RMSE between observed and modeled PM_{2.5}. The PM_{2.5} enhancements are simulated using the Stochastic Time-Inverted Lagrangian Transport (STILT) model driven with several fire emission inventories.

²Correlation and RMSE between observed and modeled PM_{2.5}. Here the results from STILT are combined with local observed meteorology from sondes (precipitation, wind speed, wind direction, mixing height) and fit to the observed PM_{2.5} enhancements using the least absolute shrinkage and selection operator (LASSO), a form of regularized linear regression.

Table 2: The percentage of the maximum PM_{2.5} simulated STILT enhancements to corresponding total observed PM_{2.5} for each burning season in Delhi during 2012-2016. OBS refers to the range of PM_{2.5} enhancements derived using the three baseline methods (see section 3.1). Each of the other columns reports simulated PM_{2.5} enhancements from STILT.

Year	Maximum enhancement					
	OBS ¹	GFED	GFED+AGRI ²	QFED	FINN	GFAS
2012	21-60%	13%	40%	33%	38%	12%
2013	54-61%	15%	48%	45%	54%	24%
2014	36-50%	24%	78%	18%	68%	7.0%
2015	21-56%	19%	62%	58%	42%	15%
2016	52-72%	16%	50%	16%	34%	7.3%

¹OBS corresponds to the network-averaged PM_{2.5} enhancement that was observed on same day that the maximum STILT-simulated PM_{2.5} enhancement occurred.

²GFED+AGRI is an emissions inventory based on GFED dry matter emissions, with 100% agriculture landcover assumed and emissions factors increased by a factor of three.

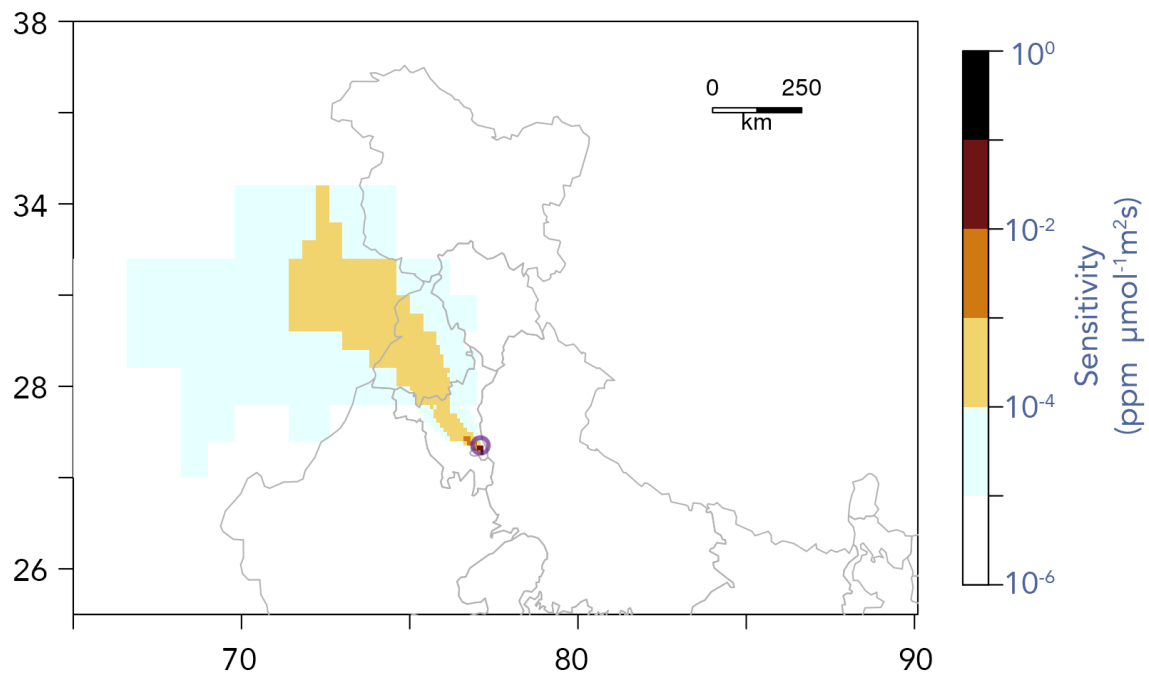


Figure 1: Median 2012-2016 STILT sensitivity of Delhi (28.62N, 77.21E, purple circle) PM_{2.5} observations to surrounding fire emissions during the post-monsoon burning season (Oct. 17 - Nov 30). Sensitivities below 10^{-6} ppm $\mu\text{mol}^{-1} \text{m}^2 \text{s}$ are not shown.

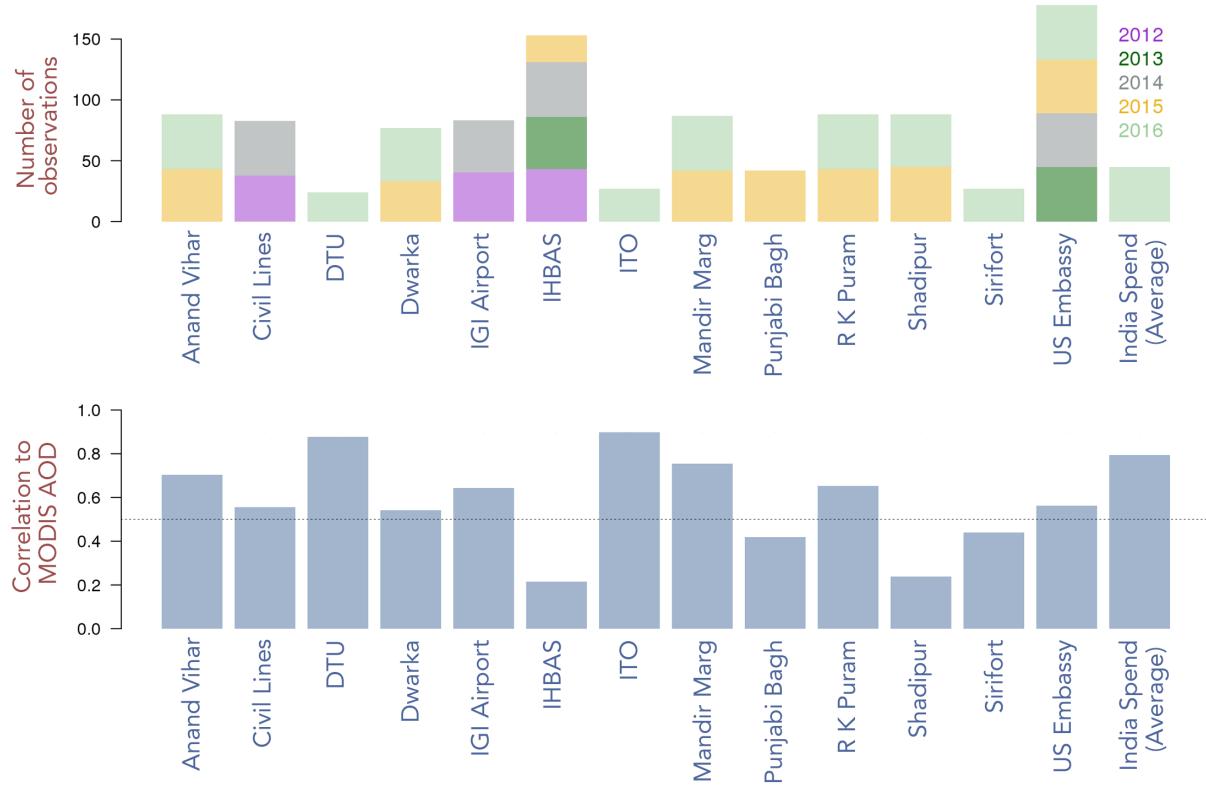


Figure 2: (Top) Number of daily-averaged $\text{PM}_{2.5}$ observations available at the Central Pollution Control Board (CPCB), U.S. Embassy, and India Spend sites for each year during 2012-2016. (Bottom) Correlations R between observed $\text{PM}_{2.5}$ and satellite aerosol optical depth (AOD) over Delhi. The horizontal line at $R = 0.5$ corresponds to the threshold used to determine if a site is included in the $\text{PM}_{2.5}$ network average. All correlations above $R = 0.5$ are statistically significant ($p < 0.05$).

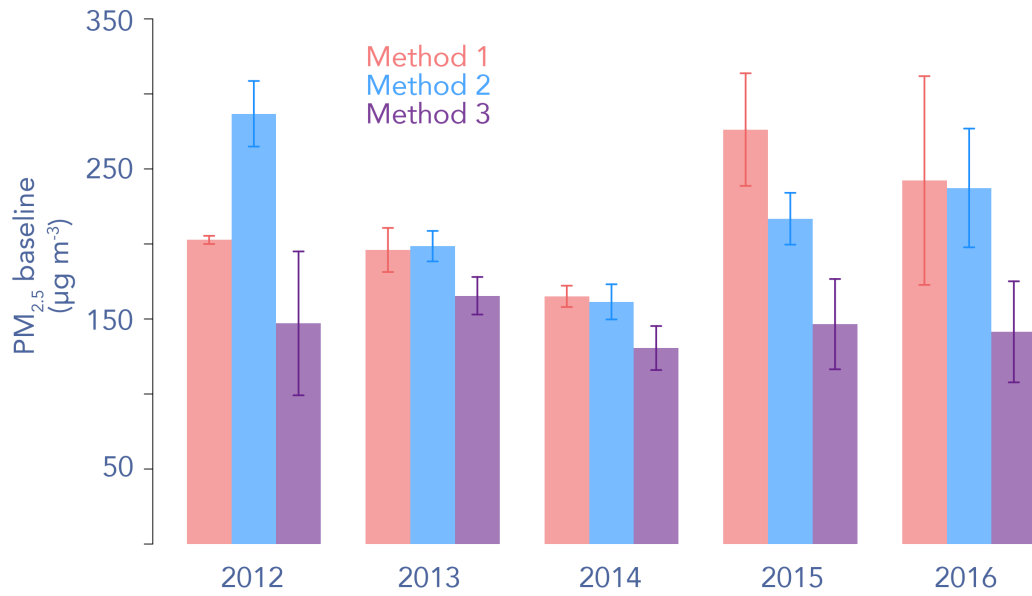


Figure 3: Estimates of the anthropogenic PM_{2.5} background in Delhi during the burning season (Oct. 17 – Nov. 30). Method 1 determines the baseline by averaging all observations on the last day of N days of no fires in the Punjab. Method 2 compares overlapping fire and STILT sensitivity grid cells, and determines a baseline if little or no overlap is detected. Method 3 averages the lowest M weekly average PM_{2.5} observations. Error bars represent 1 standard deviation when baseline parameters (e.g., N, M) are varied, as described in the text.

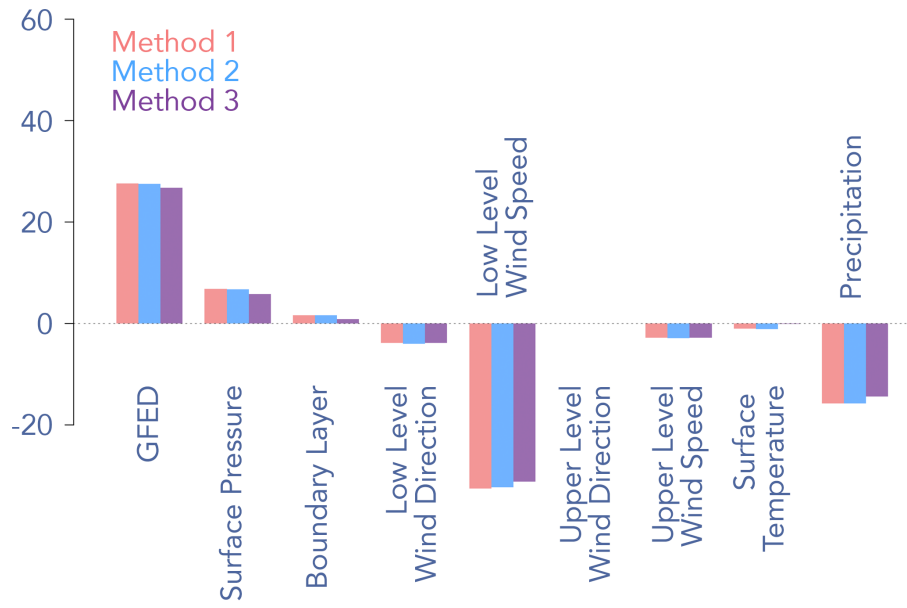


Figure 4: Standardized regression coefficients ($\mu\text{g m}^{-3}$ standard deviation $^{-1}$) fit to daily PM_{2.5} enhancements, derived from three different baseline methods. See text for description of these methods. The GFED term is the PM_{2.5} prediction based on driving STILT with GFED4.1s. The other predictors are derived from surface or sonde observed meteorology.

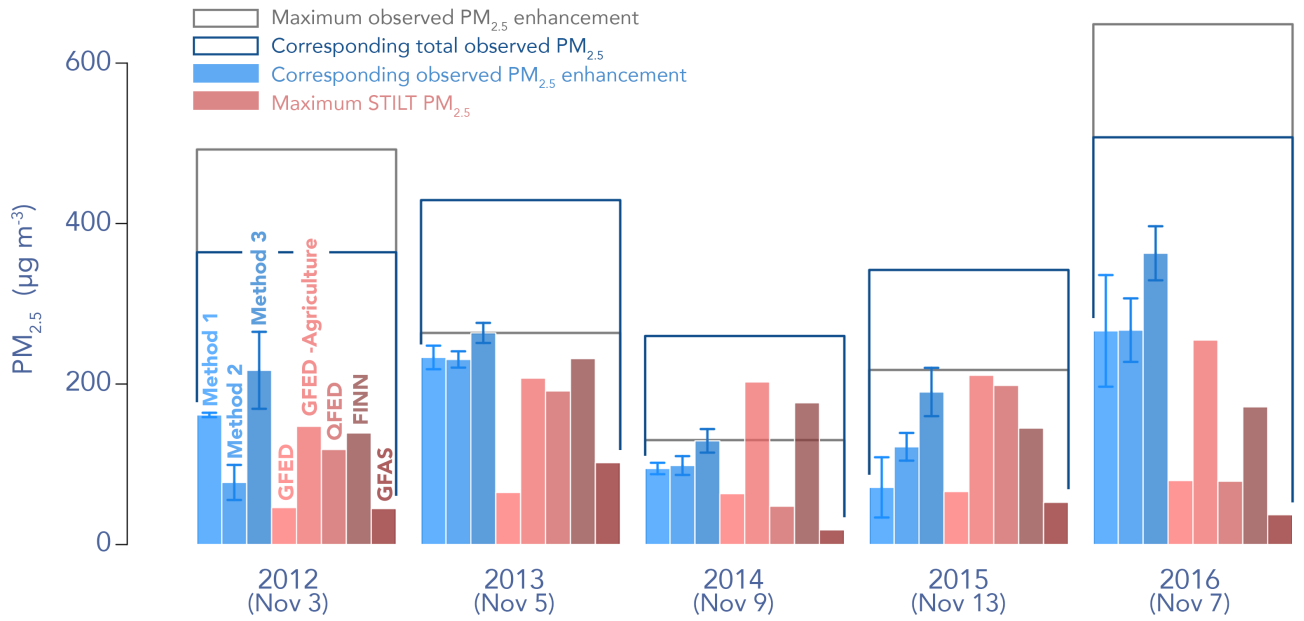


Figure 5: The maximum of daily simulated enhancements of $\text{PM}_{2.5}$ due to fires upwind fires during each post-monsoon burning season. In parentheses is the day in which the STILT simulation of $\text{PM}_{2.5}$ reached its maximum during each burning season from 2012-2016. In shades of red are the different model simulated $\text{PM}_{2.5}$ enhancements using different fire emission inventories that correspond to the date in parentheses. In shades of blue are the different network-averaged observed $\text{PM}_{2.5}$ enhancement estimates above the anthropogenic baseline for three different baseline methods that correspond to the date in parentheses. The outlined dark blue box represents the total observed $\text{PM}_{2.5}$ for the date in parentheses. The outlined grey box represents the maximum observed $\text{PM}_{2.5}$ enhancement regardless of the date when the STILT simulation predicted largest enhancement during the post-monsoon burning season.

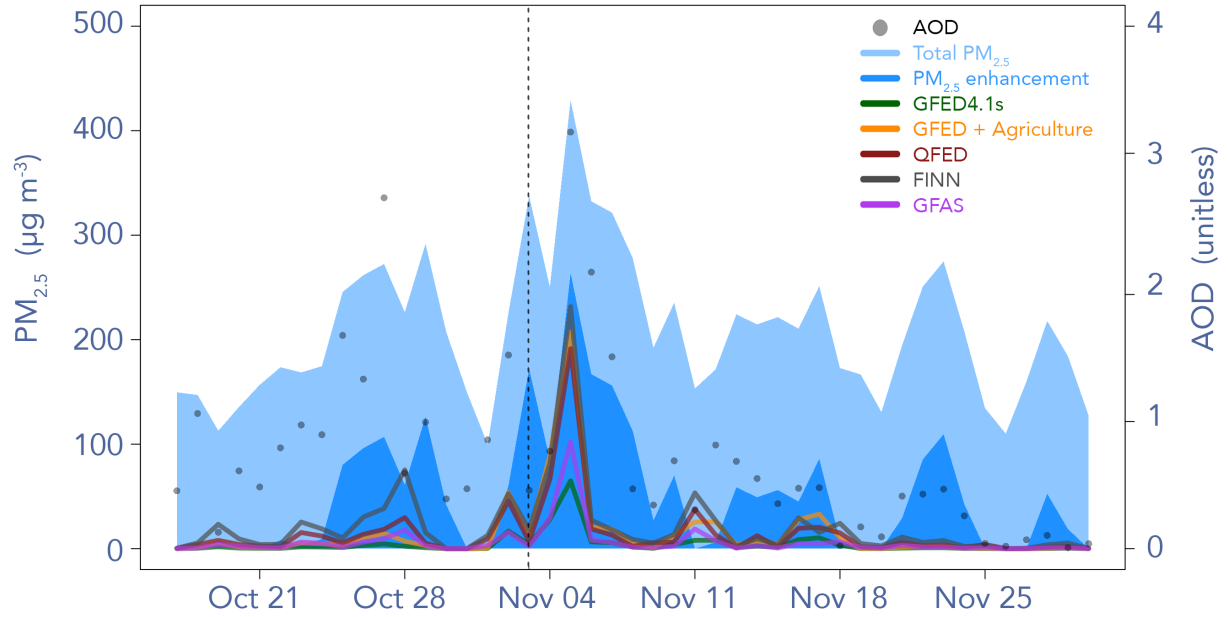


Figure 6: Time series of observed and modeled $\text{PM}_{2.5}$ during the 2013 burning season. The blue envelopes represent the observed total $\text{PM}_{2.5}$ and the $\text{PM}_{2.5}$ enhancement derived by subtracting the daily $\text{PM}_{2.5}$ by the mean $\text{PM}_{2.5}$ of the lowest week during the season. Each colored line represents a model simulation with a different fire emission inventory. The black dots are the MODIS AOD retrievals during the burning season. The dashed vertical line on represents the start of the Diwali festival for 2013 (Nov. 3rd).

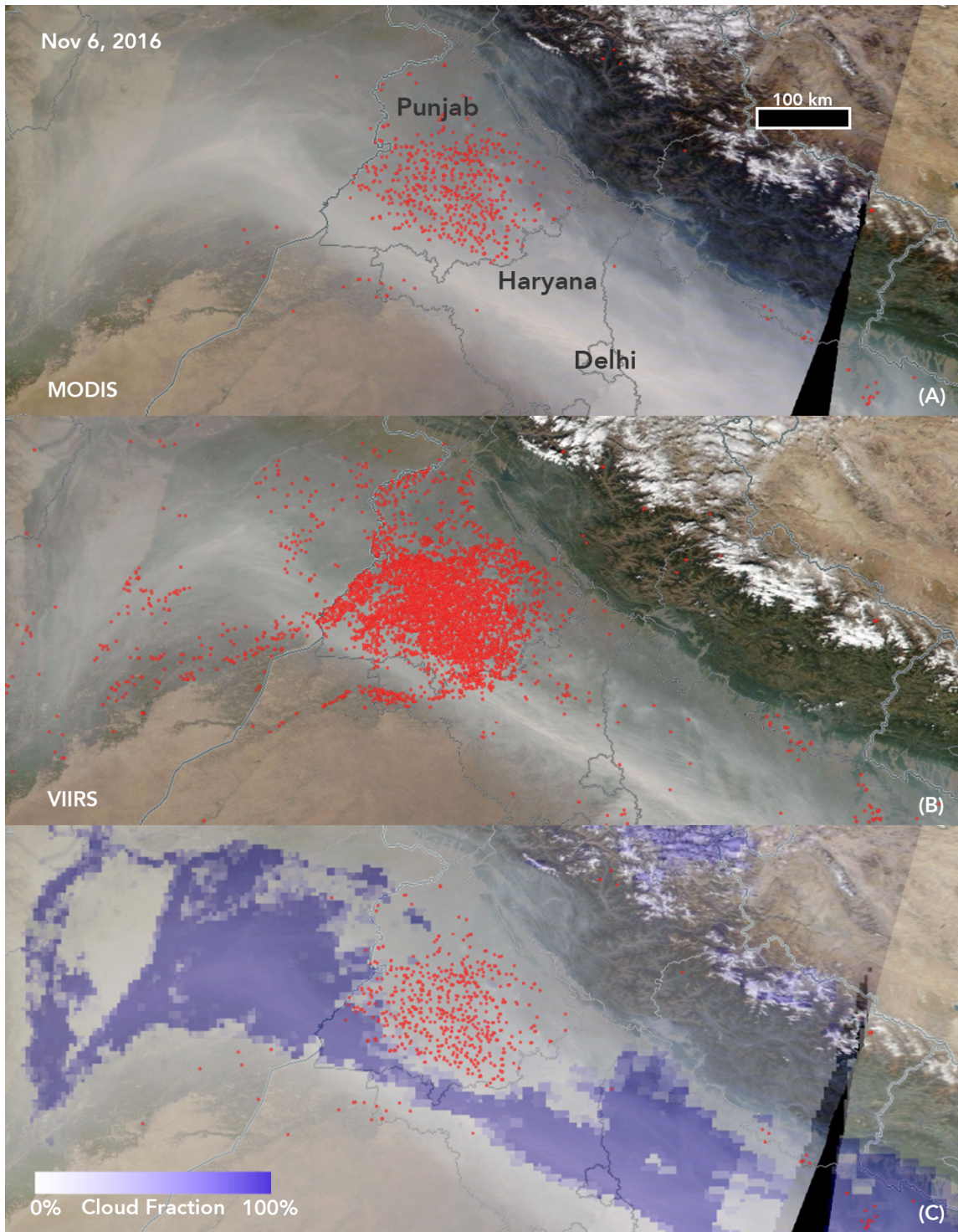


Figure 7: MODIS or VIIRS surface reflectance maps for November 6, 2016 overlaid with different fire and cloud detection algorithms. The top panel (A) shows the Terra and Aqua MODIS 1 km fire counts used in part to drive the fire emission inventories used in this paper. The middle panel (B) shows 375 m VIIRS day and night fire detections. The third panel (C) shows MODIS fire detections with MODIS Terra daytime cloud fraction overlaid. Comparison of the top and middle panels show that the resolution of the satellite sensor could influence the number of fires detected,

meaning that many smaller fires may be undetected with current MODIS capabilities. Comparison with the bottom panel shows that thick smoke in the Indo-Gangetic Plain may be detected as clouds, which may interfere with surface thermal anomalies.

Supplementary Figures

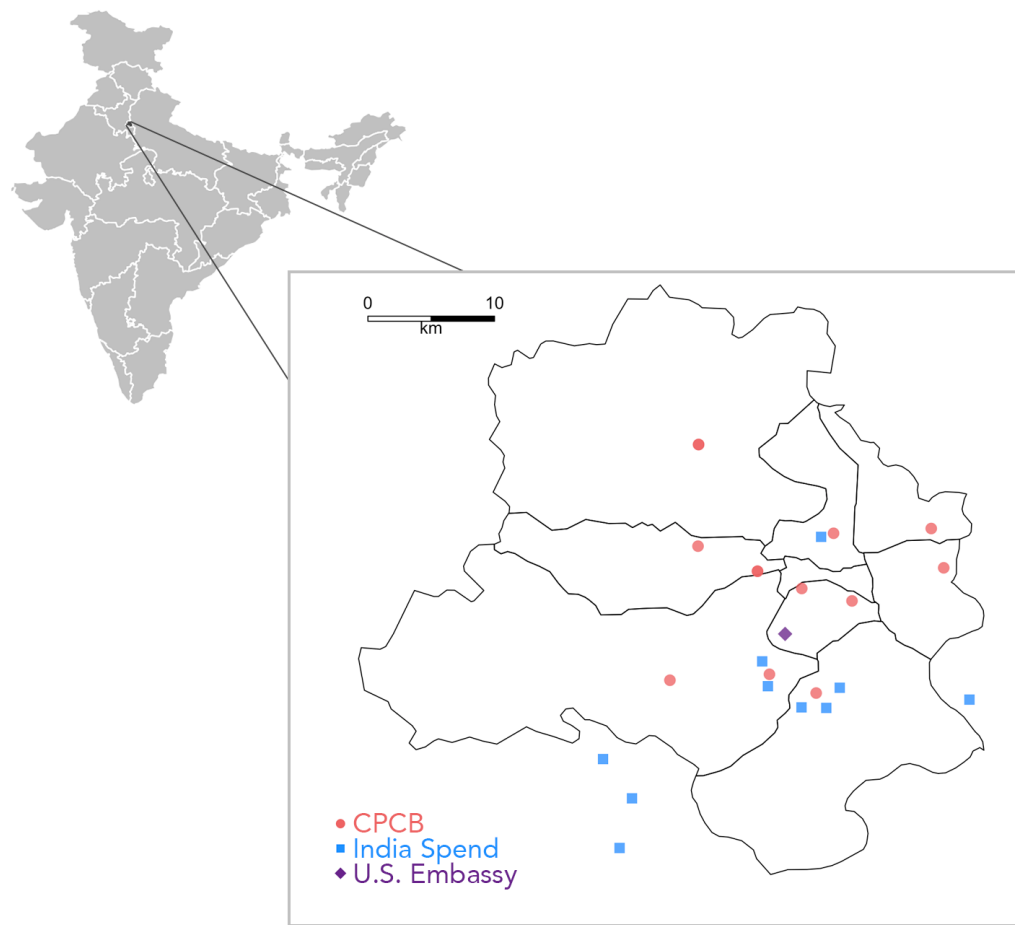


Figure S1: Distribution of Central Pollution Control Board (CPCB), India Spend, and U.S. Embassy PM_{2.5} monitoring sites located in and around the Delhi. Solid lines represent districts within the National Capital Territory of Delhi.

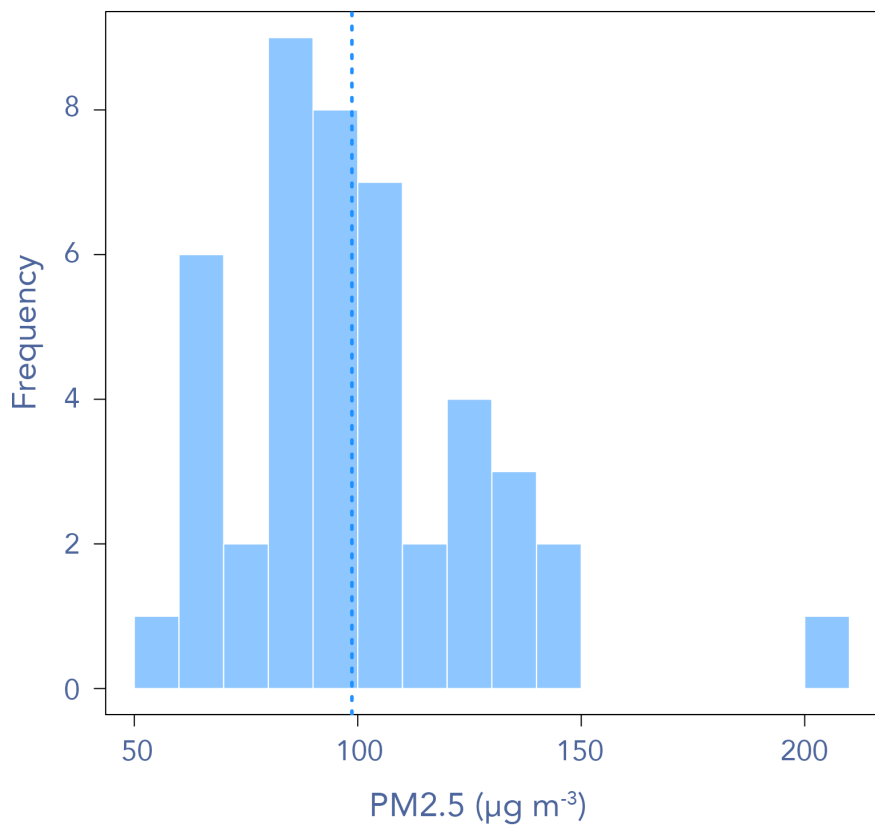


Figure S2: Frequency of PM_{2.5} daily observations in Delhi derived from a GEOS-Chem simulation performed at 0.5° x 0.667° horizontal resolution during the burning season of 2012 (Oct 17. – Nov. 30). The dashed vertical line represents the mean of the distribution.

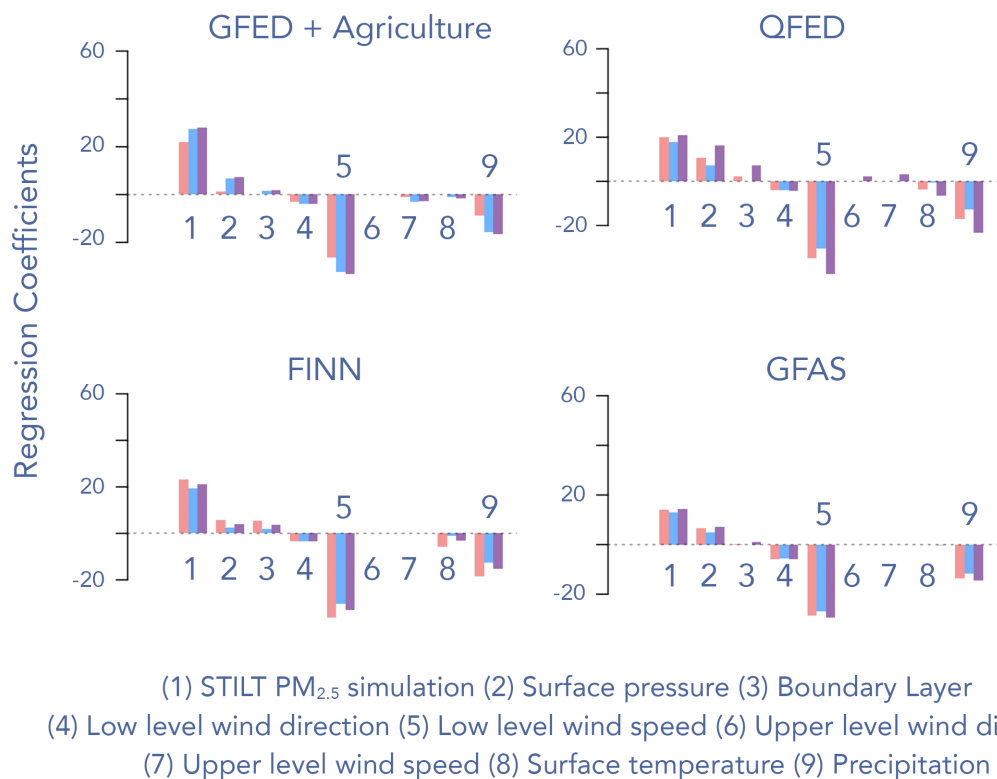


Figure S3. Standardized regression coefficients ($\mu\text{g m}^{-3}$ standard deviation $^{-1}$) fit to daily PM_{2.5} enhancements, derived from three different baseline methods. See text for description of these methods. The first term, labeled “1, STILT PM_{2.5} simulation,” represents simulated PM_{2.5} using one of four fire emission inventories – GFED + Agriculture, which assumes 100% agricultural landcover and emission factors increased by a factor 3; QFED; FINN; and GFAS.

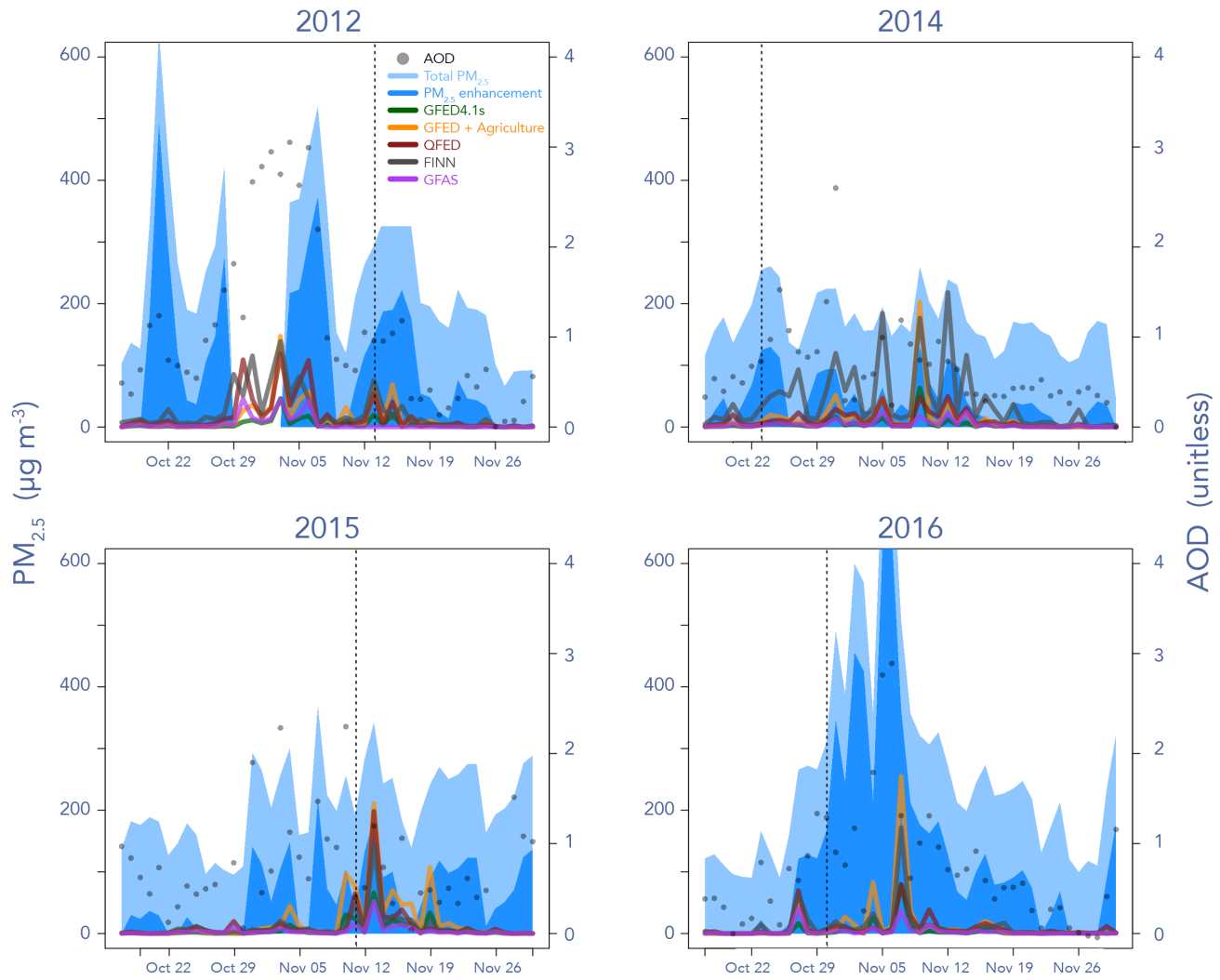


Figure S4: Time series of observed and modeled $\text{PM}_{2.5}$ during the 2012, 2014-2016 post-monsoon burning seasons. The blue envelopes represent the observed total $\text{PM}_{2.5}$ and the $\text{PM}_{2.5}$ enhancement derived by subtracting the daily $\text{PM}_{2.5}$ by the mean $\text{PM}_{2.5}$ of the lowest week during the season. Each colored line represents a model simulation with a different fire emission inventory. The black dots are the MODIS AOD retrievals during the burning season. The dashed vertical lines represent the first day of the Diwali festival.